19e Journées de l'Hydrodynamique
26 – 28 novembre 2024, Nantes

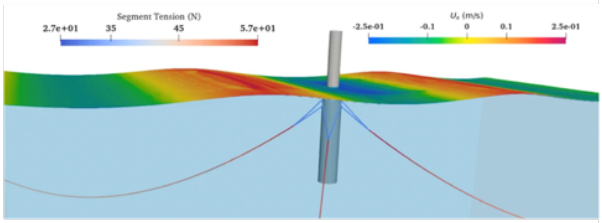

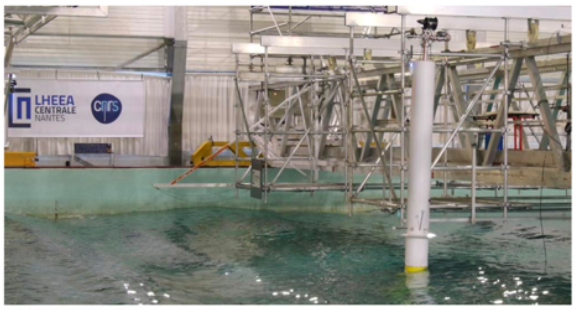

CARACTERISATION NUMERIQUE ET EXPERIMENTALE DES STATISTIQUES DE VAGUES DEFERLANTES

NUMERICAL AND EXPERIMENTAL WAVE BREAKING CHARACTERIZATION

M. YATES[(1)], S. MOHANLAL[(1,2)], J. HARRIS[(1)], J. WANG[(1)], L. PASTUR[(3)], C. PEYRARD[(1)], S. GRILLI[(4)]

marissa.yates@enpc.fr ; s.mohanlal@hrwallingford.com ; jeffrey.harris@enpc.fr ; jiankai.wang@enpc.fr ; luc.pastur@ensta-paris.fr ; christophe.peyrard@edf.fr ; grilli@uri.edu

[(1)]LHSV, École des Ponts, EDF R&D, Chatou, France
[(2)]Coasts & Oceans, HR Wallingford, Wallingford, Oxfordshire, UK
[(3)]Unité de Mécanique, ENSTA Paris, IPParis, Palaiseau, France
[(4)]Department of Ocean Engineering, University of Rhode Island, Narragansett, RI, USA

Résumé

La caractérisation des vagues, et notamment des vagues déferlantes, est un élément essentiel pour le dimensionnement des éoliennes en mer afin d'estimer les charges maximales associées aux ULSs ("Ultimate Limit States") et la fatigue durant la durée de vie de la structure. Afin de bien représenter les états de mer sévères, il est important de prendre en compte les effets non-linéaires des vagues, ce qui nécessite une représentation précise de leur propagation. Les modèles de propagation de vagues utilisés pour le dimensionnement des éoliennes en mer devront être suffisamment efficaces pour effectuer les centaines de simulations des DLCs ("Design Load Cases") qui sont nécessaires pour évaluer l'intégrité des structures face à une gamme de différentes conditions environnementales. Dans le cadre du projet 3DWaveBI ("3D Wave Breaking Impacts"), l'objectif est d'améliorer la modélisation numérique de la propagation et du déferlement des vagues, et aussi l'estimation des efforts des vagues sur les structures, pour des états de mer irréguliers ayant des vagues non-linéaires et déferlantes. Pour valider les approches de modélisation de vagues proposées, il est nécessaire d'obtenir des observations adéquates, en particulier en 3 dimensions. Ce projet répond à ce besoin de mesures expérimentales de la propagation des vagues, en se focalisant sur l'évaluation de l'impact d'une bathymétrie variable. Cet article présente brièvement une partie des travaux numériques réalisés dans la première phase de ce projet, avant de présenter les données acquises pendant des essais en laboratoire réalisés récemment dans un basin à vagues 3D, dans la deuxième phase du projet.

Abstract

The characterization of the wave field, and in particular breaking waves, is an essential element in the design of offshore wind turbines to estimate both the structural fatigue during its lifetime and the maximum loads associated with Ultimate Limit States (ULSs). To represent well severe wave states, it is necessary to estimate nonlinear wave effects, which requires having accurate knowledge of the wave field. Models used in offshore wind turbine design must be efficient to be able to run hundreds of simulations of Design Load Cases (DLCs) that are used to assess the loads on the structure to ensure its integrity facing a range of different environmental conditions. In the 3D Wave Breaking Impacts (3DWaveBI) project, the objective is to improve numerical modeling of wave propagation and breaking, as well as the estimation of wave loads on structures in irregular sea states, including highly nonlinear and breaking waves. There is a need for observations, in particular in 3D settings, to validate a range of wave modeling approaches. Thus, this project complements numerical modeling studies with experimental measurements of wave propagation, with a particular focus on investigating the impacts of a variable bottom bathymetry. This paper briefly summarizes some of the model development achieved in the first phase of the project, and outlines the data acquired during recent experiments completed in a 3D wave basin in the second phase of the project.

I – Introduction

With the rapidly accelerating growth of the offshore wind industry, there is a strong need for an improved characterization of the most extreme offshore wave fields, notably including breaking waves. This is necessary to estimate both the fatigue and ultimate loads expected during a structure's lifetime. In the design phase of offshore wind farms, a range of modeling tools are used to estimate the structure's response to a wide variety of environmental conditions specified by design standards. In particular, highly efficient and accurate wave models are needed to simulate the local wave conditions around a structure and to estimate the wave impacts on the structure.

To simulate accurately wave breaking processes and the wave breaking loads on structures, recent work has progressed significantly in the development of two-phase CFD (Computational Fluid Dynamics) models simulating the air-wave-structure interactions, e.g., [10, 16]. These models are highly accurate at local, near-field scales, but are limited in their spatial domain size. Thus, they often simulate focused breaking waves, which may not represent well the wave geometry and associated impact forces of irregular waves in a natural sea state [18]. Therefore, more efficient models are also needed to simulate irregular sea states that are representative of natural wave conditions, such as using Boussinesq-type [19, 11] or Fully Nonlinear Potential Flow (FNPF) (using finite difference e.g., [3], Boundary Element Method (BEM), e.g. [8], High-order spectral (HOS), e.g. [20]), or similar methods. These phase-resolving models do not allow simulating explicitly wave breaking events, but do allow simulating the far-field wave conditions and estimating accurately nonlinear wave characteristics and kinematics of irregular sea states. In recent years, much attention has been given to improving estimates of the parameterization of wave breaking in phase-resolving wave models, focused primarily on the identification of breaking onset and the estimation of the induced wave energy dissipation, e.g. [11, 2, 20, 6].

To validate models used in offshore wind turbine design, observations of wave propagation and the associated loads on structures, in particular in 3D settings, are necessary

[1]. In addition, the majority of existing laboratory studies in two-dimensional (2D, canal) or three-dimensional (3D, basin) settings were completed with a flat bottom, but [4] demonstrated that a variable bathymetry can have important impacts on wave breaking processes. They showed that bathymetric effects may increase the curling factor, to which wave loads are proportional, and this increase may be particularly significant during the most penalizing slamming events. Recent projects measuring irregular, uni- and multi-directional waves in 3D wave basins and the resultant loads on structures were conducted in the DeRisk [17] and Floatech [12] projects for flat bottom bathymetries. Thus, the objective of our recent 3DWaveBI (3D Wave Breaking Impacts) project is to respond to the need to improve the characterization of waves, wave breaking and their impacts on structures, by experimentally and numerically evaluating wave transformation, breaking, and impacts on structures for variable bottom bathymetries.

The initial aim of the first phase of this project focused on the implementation and improvement of 2D and 3D FNPF modeling of wave propagation and breaking, using existing laboratory measurements to validate the modeling approach [13, 15]. The second phase of the project consisted in laboratory experiments that were completed in a 3D wave basin with 4 principal objectives : (1) the characterization of wave transformation over a variable bathymetry, (2) the identification of wave breaking zones at the free surface, (3) the characterization of the type of wave breaking for major breaking events, and (4) the measurement of breaking wave loads on a cylindrical structure. An overview of the laboratory experiments will be presented here, showing preliminary analyses in progress.

II – Numerical model

The 2D version of the fully nonlinear potential flow (FNPF) model Misthyc [22, 13] was used to simulate the propagation of waves over 2D cross-shore transects extracted from the dune bathymetry (profiles B and C in Figure 1b) in the laboratory experiments. By assuming an inviscid and incompressible fluid and irrotational flow, the velocity potential $\phi(x, z, t)$ satisfies the Laplace equation in the fluid domain. By additionally assuming a single-valued free surface, the kinematic and dynamic free surface boundary conditions (also known as the Zakharov equations [23]) can be written as :

$$\eta_t = -\nabla\eta \cdot \nabla\tilde{\phi} + \tilde{w}(1 + \nabla\eta \cdot \nabla\eta) \quad (1)$$

$$\tilde{\phi}_t = -g\eta - \frac{1}{2}\nabla\tilde{\phi} \cdot \nabla\tilde{\phi} + \frac{1}{2}\tilde{w}^2(1 + \nabla\eta \cdot \nabla\eta) - \frac{p_a}{\rho}, \quad (2)$$

where $\eta(x, t)$ is the free surface position, $\tilde{\phi}(x, t) = \phi(x, \eta(x, t), t)$ is the free surfance velocity potential, $\tilde{w}(x, t) = \frac{\partial\phi}{\partial z}|_{z=\eta}$ is the free surface vertical velocity, and p_a is the atmospheric pressure, which is typically set to 0. At the bottom, an impermeable boundary condition is applied, and at the vertical boundaries, either Dirichlet or wall boundary conditions are applied in wave generation and absorption zones, respectively. The coordinate system is transformed to a fixed rectangular domain using sigma coordinates. High-order finite difference schemes are used in the horizontal, and a spectral approach expressing the velocity potential as a sum of Chebyshev polynomials is used in the vertical. This assumption, along with the assumption of potential flow, prevents being able to simulate explicitly the overturning of the free surface and wave breaking.

The model currently defines breaking onset using the criterion $B = u/c = 0.85$, first proposed by [2] for deep and intermediate water conditions, and then validated by [6] in shallow water conditions. Wave energy dissipation is applied as a local damping pressure,

p_a in Eq.(2), following [9]. [13] validated this approach in Misthyc, showing good agreement for both regular and irregular wave propagation and breaking over barred and sloped bathymetric profiles.

III – Experimental setup

Laboratory experiments were conducted in a 30-m wide by 25-m long section of the 3D wave basin in the EDF Lab Chatou experimental hall. The physical model was designed to represent a variable bottom bathymetry in the form of a submarine dune at a scale of 1/40. Two constant slope faces of the dune are oriented such that they are exposed to incident waves generated by the snake-type wavemaker (Figure 1a). Waves propagating at -30° (using the convention of 0° being perpendicular to the wavemaker) pass over a 1/25 slope, and at +15° over a 1/12 slope. The back and far side of the dune have the steepest slopes of 1/2.

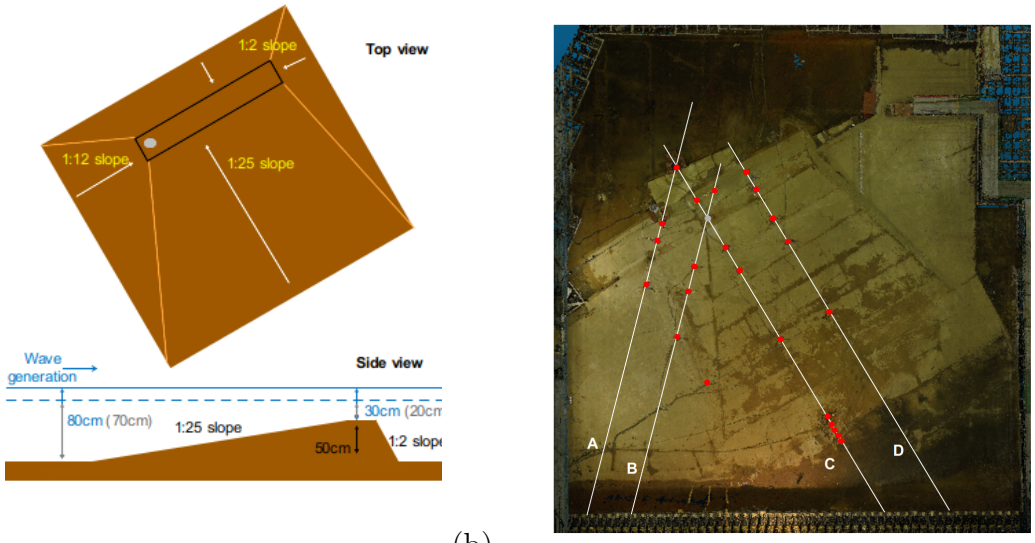

(a) (b)

FIGURE 1 – Bathymetry and setup of the experiments : (a) schematic of the top and side views of the schematic dune profile indicating the shape, orientation, water depth, and position of the monopile (gray circle), and (b) photogrammetric drone survey of the wave basin showing the position of the dune relative to the wavemaker (bottom) and wave absorbers (majority of the three remaining walls). The monopile (gray circle in both plots, located at the intersection of profiles B and C in the right plot), wave gauges and associated transects A-D (red circles and white lines in the right plot) are indicated.

A drone survey of the wave basin was completed using photogrammetry to measure the bathymetry, showing the 25-m long wavemaker consisting of 56 paddles and the wave absorbers spanning the majority of the 3 remaining sides of the tank (Figure 1b). Eighteen resistive wave gauges measured the free surface position throughout the wave basin (red points, with one non-functioning gauge). An additional 5 wave gauges were aligned in front of the wavemaker (oriented following the incident wave direction for the unidirectional wave cases) to measure the generated incident wave field and the observed wave reflections (e.g. setup for -30° waves shown in Figure 1b). The wave gauges were placed along 4 profiles : 2 aligned with the +15° slope (A and B) and 2 aligned with the -30° slope (C and D). The cylindrical structure representing a monopile was positioned near the end

of the flat crest of the dune (intersection of profiles B and C) such that waves breaking on the monopile propagated up the slopes oriented at +15 and -30° (aligned with the profiles), as well as over a more variable slope at 0° wave incidence.

A Froude number scaling was used to estimate the wave conditions and diameter of the cylindrical structure (22.7 cm, corresponding to a full scale monopile with a diameter slightly larger than 9 m). One aim of this project is to evaluate the type of wave breaking, distinguishing between spilling and plunging breaking waves, since plunging waves may generate significant forces on offshore structures during slamming events. The characterization of wave breaking types is typically estimated as a function of the surf similarity parameter, also known as the Iribarren or Battjes number, ξ_0. It is defined as $\xi_0 = S/\sqrt{H_0/L_0}$, where S is the average bottom slope, and H_0 and L_0 are the deep water wave height and wavelength, calculated as $L_0 = gT/4\pi$. Spilling breaking waves typically have $\xi_0 < 0.5$, and plunging breaking typically fall in the range of $0.5 < \xi_0 < 3.3$. To test the use of the surf similarity parameter to characterize and quantify wave breaking statistics and impacts, a range of significant wave heights and wave periods were tested at 2 water levels, and three incident wave directions. Table 1 summarizes the range of values of full scale and laboratory conditions tested in the experiments. Unidirectional, irregular waves were generated with the snake-type wavemaker using a JONSWAP wave spectrum with a peak enhancement factor of 3.0, theoretical values of $H_{s,theor}$ and $T_{p,theor}$, and measured incident values of $H_{s,meas}$ and $T_{p,meas}$. Multidirectional, irregular waves were also generated for a limited number of test cases with constant H_s, T_p, and water depth, with a mean incident direction of 0°, and several different directional spreading functions.

Test case parameters	Laboratory scale	Full scale
h [m]	0.7-0.8	28-32
$H_{s,theor}$ [m]	0.075-0.2	3.0-8.0
$H_{s,meas}$ [m]	0.076-0.182	3.0-7.28
$T_{p,theor}$ [s]	1.11-1.9	7.02-12.02
$T_{p,meas}$ [s]	1.08-1.86	6.81-11.78
S [-]	1/25-1/12	
θ [°]	+15, 0, -30	

TABLE 1 – Test case parameters at the laboratory and full scales : water depth h, bottom slope S, theoretical significant wave height and peak period $H_{s,theor}$, $T_{p,theor}$, measured significant wave height and peak period $H_{s,meas}$, $T_{p,meas}$, and incident wave direction θ (relative to 0° perpendicular to the wavemaker).

In addition to the wave gauge measurements of the free surface position, two cameras were installed with a top and side view of the wave basin. A high resolution camera (25 Megapixel Vieworks monochrome camera, 5120 by 5120) was installed in the ceiling of the laboratory, approximately 13 m above the wave basin, with a view of the free surface to identify wave breaking events by the presence of foam generated during wave breaking. A high-speed Photron Mini UX50 monochrome camera was installed on the bridge adjoining the wave basin to record wave breaking events impacting the monopile. The Photron camera acquisition was synchronized with a multiaxes AMTI load cell (Version IP 68) that was installed in the monopile, measuring the three force and three moment components.

IV – Results and discussion

IV – 1 Numerical modeling of the laboratory experiments

Leading up to the experiments, a series of 2D numerical model runs were completed to evaluate the test conditions and to estimate the location of wave breaking events. The aim was to select a range of wave conditions spanning different values of the surf similarity parameter, also generating wave breaking on the two slopes of the dune and at the crest. The goal was to ensure that a full range of non-breaking and breaking events, including different phases of wave breaking at the monopile would be recorded during the laboratory experiments. Therefore, model simulations were run for the range of proposed test cases to identify the presence, intensity, and spatial range of expected breaking events (e.g. Figure 2, for $H_s = 0.125$ m, $T_p = 1.42$ s, $h = 0.7$ m, and $\theta = -30°$. The energy dissipa-

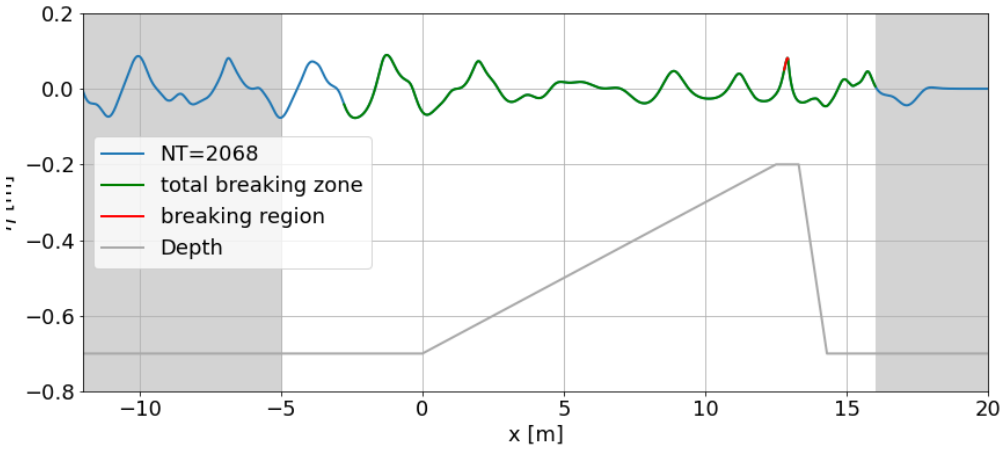

FIGURE 2 – Misthyc model test run showing a snapshot (at timestep NT=2068, with $dt = 0.02$ s, and a $CFL = 1$) of the free surface position in the model domain (blue) with a wave breaking event in progress identified in red. The green curve indicates the full extent of the surf zone for this test case with a Jonswap spectrum with $H_s = 0.125$ m and $T_p = 1.42$ s, and $h = 0.7$ m, for a simulation lasting 6 minutes.

tion applied during breaking events depends on the non-dimensional parameter b, which represents the intensity of wave breaking and is estimated as a function of the temporal derivative of B, dB/dt, as shown by [5] in intermediate and deep water conditions. [13] proposed that $b = 0.05$ is a reasonable (constant) approximation of the mean value of b during breaking events in shallow water, therefore simplifying the calculation of the energy dissipation of a breaking wave. Using data from 5 sets of experiments over barred and constant slope bathymetries, the authors additionally observed that dB/dt appears to be related to the type of wave breaking (Figure 3). Following [5], they showed that the onset strength $\gamma = T_b \frac{dB}{dT}|_{B=B_{th}}$, where T_b is the wave period at breaking and B_{th} is threshold value of B (0.85), may be able to be used to distinguish between spilling and plunging wave breaking events. They observed a transition between spilling and plunging breakers in the range of $\gamma = 1.3 - 1.4$, but suggested that a larger number of test cases must be evaluated to verify this hypothesis. This is one of the ongoing objectives of the simulation runs and data analysis of the type of wave breaking observed in the experiments.

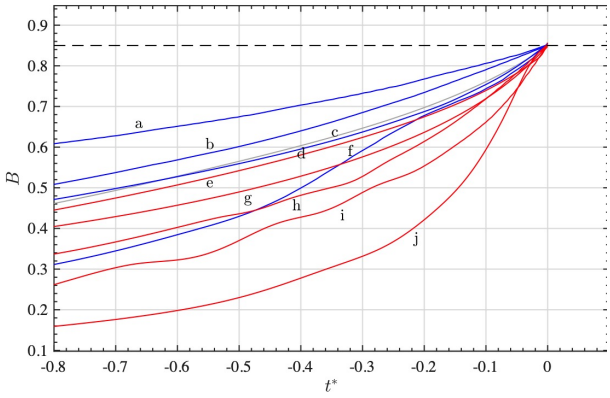

test	ξ_0	γ
a	0.118	0.77
b	0.202	0.80
c	0.394	1.01
d	0.208	1.12
e	0.520	1.54
f	0.744*	1.30
g	0.499*	1.65
h	0.569	1.43
i	0.672	2.47
j	0.894	1.52

FIGURE 3 – (left) Evolution of B as a function of the nondimensional time $t^* = (t - t_b)/T_b$, where t_b is the wave breaking onset and T_b is the wave period at breaking (Fig. 16 of [14]). (right) The color of the surf similarity parameter ξ_0 and onset intensity γ corresponds to the type of wave breaking observed in the experiments : spilling (blue) and plunging (red), where the stars indicate differences with the threshold values of ξ_0.

IV – 2 Wave breaking identification

The high resolution camera recorded the 25-minute long experimental runs with the objective of identifying the wave breaking zones by the presence of foam on the free surface. This technique has been used previously in field studies (e.g. [21, 7]) and is applied here to identify the wave breaking zones throughout the wave basin, including the onset and termination of breaking events, as well as the overall wave breaking statistics for each sea state. This data set can then be used to validate phase-resolving 3D wave propagation models and, in particular, the implementation of wave breaking in these types of models, such as the model proposed in the first phase of the 3DWaveBI project (e.g. [15]).

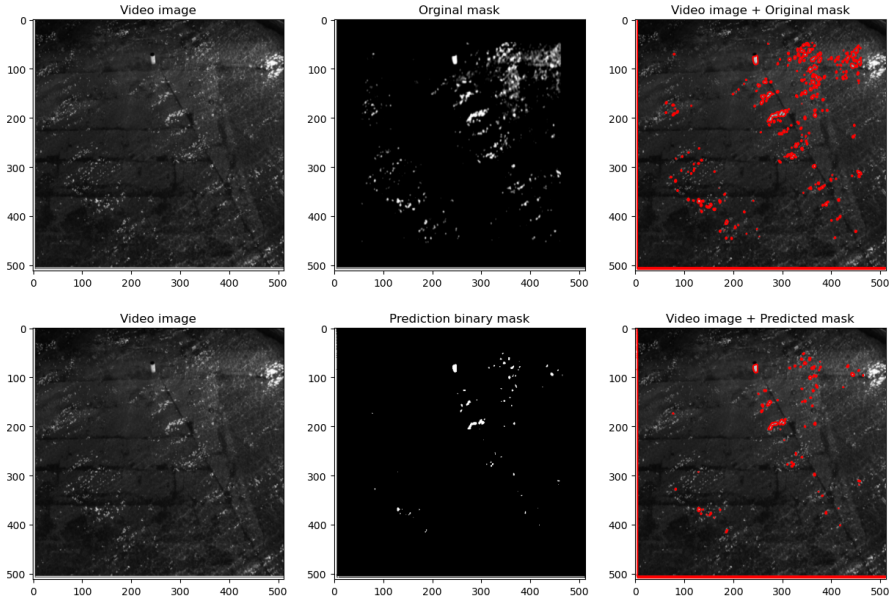

FIGURE 4 – Example of the application of the "classic" approach (top row) and U-Net (bottom row), showing the original image (left), masks (center), and identified breaking zones (red, right). (Note the illustrations are the mirror image of the wave basin.)

To extract the wave breaking zones from the images, two image analysis techniques have been implemented : (1) a "classic" segmentation approach that is based on several steps of filtering, thresholding, and clustering (e.g. Figure 4, top row), and (2) a segmentation approach using a U-net convolutional neural network to improve the efficiency of the analysis to enable analyzing a large number of images (e.g. Figure 4, bottom row). The preliminary results show the ability to identify and cluster bright zones in the images, but work in progress remains to succeed in distinguishing between areas with foam and with reflections of light from the experimental hall.

IV – 3 Wave breaking classification

The high-speed camera installed with a side view including the monopile and a small zone of wave propagation leading up to the monopile, allows classifying the observed type of wave breaking for a selection of breaking events. Due to limitations in the data storage capacity of the camera when it is synchronized with the load cell, it is possible to record approximately 36 seconds at a frequency of 250 i/s during each experiment. This allows showing high temporal resolution details of the progression of each non-breaking and breaking wave event (e.g. Figure 5). These images are synchronized with the load cell measurements that were recorded at 2000Hz to capture the sharpest peaks in the wave loads. Finally, these images may also be used to track the level of wave runup on the visible side of the structure during non-breaking and breaking events.

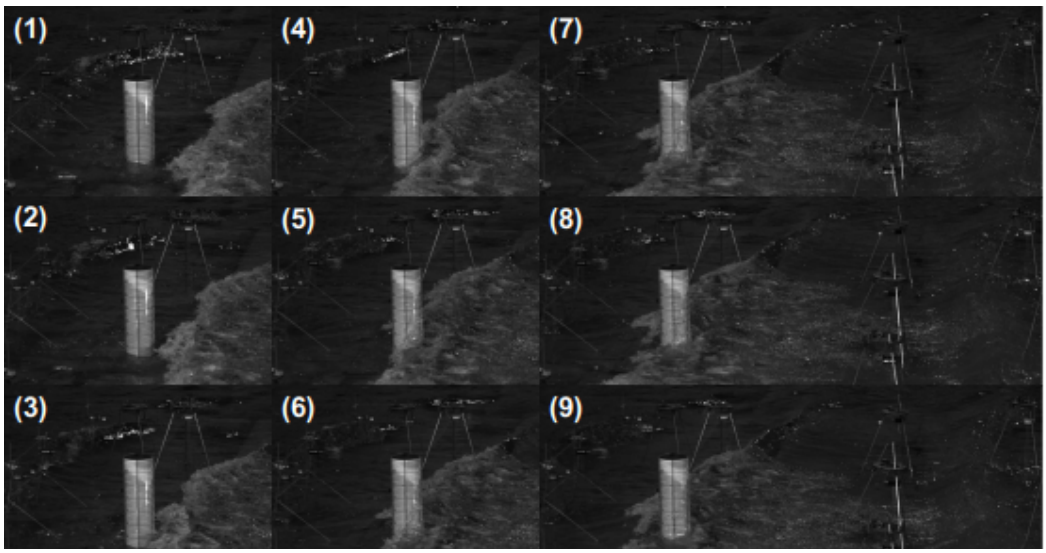

FIGURE 5 – High-speed camera images of a breaking wave at the location of the structure during test case 053, with $H_s = 0.175$ m, $T_p = 1.42$ s, $h = 0.8$ m, and $\theta = -30°$. The nine images are a selected subset at 25 Hz, covering a period of 0.32 s in total.

V – Conclusion

The 3DWaveBI project aims to advance the development of wave propagation models, including taking into account the effects of wave breaking, and to validate the proposed approaches with laboratory experiments that are unique in their focus on evaluating wave propagation over a variable bathymetry in a 3D wave basin. A summary of the previous numerical work completed in the first phase of the project is presented, identifying the need

to complete additional laboratory and numerical simulations of wave breaking events to evaluate the use of the onset intensity γ to evaluate the type of wave breaking (e.g. spilling versus plunging). Then, an overview of the recent laboratory experiments is provided to show the analysis in progress that will provide a large dataset of 3D wave propagation, breaking characterization and statistics, and impacts on structures for a range of numerical model validation purposes and applications in offshore wind turbine design.

Acknowledgments

We would like to thank all of the partners of the 3DWaveBI project, including the Cerema, EDF R&D, ENPC, ENSTA, and EDF Renewables for supporting this work, as well as the Energy4Climate Interdisciplinary Center (E4C) for financing 3 internships and laboratory equipment. The thesis work of Sunil Mohanlal (2020-2023) was produced within the framework of E4C of IP Paris and Ecole des Ponts ParisTech, which was supported by 3rd Programme d'Investissements d'Avenir [ANR-18-EUR-0006-02]. This action benefited from the support of the Chair « Challenging Technology for Responsible Energy » led by l'X – Ecole Polytechnique and the Fondation de l'Ecole Polytechnique, sponsored by TotalEnergies. Finally, we are especially grateful to Clément Buvat, Nicolas Gueguen and Kevin Botten from the LNHE of EDF R&D for their assistance, thoughtful discussions, persistence, and careful work on the completion of the experiments.

Références

[1] M. Alagan Chella, A. Tørum, and D. Myrhaug. An overview of wave impact forces on offshore wind turbine substructures. *Energy Procedia*, 20 :217–226, 2012.

[2] X. Barthelemy, M. L. Banner, W. L. Peirson, F. Fedele, M. Allis, and F. Dias. On a unified breaking onset threshold for gravity waves in deep and intermediate depth water. *J. Fluid Mech.*, 841 :463–488, 2018.

[3] H. B. Bingham and H. Zhang. On the accuracy of finite-difference solutions for nonlinear water waves. *J. Eng. Math*, 58 :211–228, 2007.

[4] E. J. de Ridder, T. Bunnik, J. M. Peeringa, B. T. Paulsen, C. Wehmeyer, P. Gujer, and E. Asp. Summary of the Joint Industry Project Wave Impact on Fixed Foundations (WiFi JIP). volume Volume 10 : Ocean Renewable Energy of *International Conference on Offshore Mechanics and Arctic Engineering*, page V010T09A081, 06 2017.

[5] M. Derakhti, M. L. Banner, and J. T. Kirby. Predicting the breaking strength of gravity water waves in deep and intermediate depth. *J. Fluid Mech.*, 848, 2018.

[6] M. Derakhti, J. T. Kirby, M. L. Banner, S. T. Grilli, and J. Thomson. A unified breaking onset criterion for surface gravity water waves in arbitrary depth. *Journal of Geophysical Research : Oceans*, 125(7) :e2019JC015886, 2020.

[7] C. Eadi Stringari, P. Veras Guimarães, J.-F. Filipot, F. Leckler, and R. Duarte. Deep neural networks for active wave breaking classification. *Scientific Reports*, 11(1) :3604, Feb. 2021.

[8] S. T. Grilli, J. Skourup, and I. Svendsen. An efficient boundary element method for nonlinear water waves. *Engng. Analysis with Boundary Elemts.*, 6(2) :97–107, 1989.

[9] S. Guignard and S. T. Grilli. Modeling of wave shoaling in a 2D-NWT using a spilling breaker model. In *Proc. 11th International Offshore and Polar Engineering*

Conference, volume 3, pages 116–123. International Society of Offshore and Polar Engineers, 2001.

[10] L. Huang, Y. Li, D. Benites-Munoz, C. W. Windt, A. Feichtner, S. Tavakoli, J. Davidson, R. Paredes, T. Quintuna, E. Ransley, M. Colombo, M. Li, P. Cardiff, and G. Tabor. A review on the modelling of wave-structure interactions based on openfoam. *OpenFOAM® Journal*, 2 :116–142, Aug. 2022.

[11] M. Kazolea and M. Ricchiuto. On wave breaking for boussinesq-type models. *Ocean Modelling*, 123 :16–39, 2018.

[12] I.-C. Kim, G. Ducrozet, V. Leroy, F. Bonnefoy, Y. Perignon, and S. Delacroix. Numerical and experimental investigation on deterministic prediction of ocean surface wave and wave excitation force. *Applied Ocean Research*, 142 :103834, 2024.

[13] S. Mohanlal, J. Harris, M. Yates, and S. Grilli. Unified depth-limited wave breaking detection and dissipation in fully nonlinear potential flow models. *Coastal Engineering*, 183 :104316, 2023.

[14] S. Mohanlal, J. C. Harris, M. L. Yates, and S. T. Grilli. Unified depth-limited wave breaking detection and dissipation in fully nonlinear potential flow models. *Coastal Engineering*, 183 :104316, 2023.

[15] S. Mohanlal, J. C. Harris, M. L. Yates, and S. T. Grilli. Simulation of depth-limited breaking waves in a 3d fully nonlinear potential flow model. *Journal of Waterway, Port, Coastal, and Ocean Engineering*, 150(4) :04024007, 2024.

[16] W. Mostert, S. Popinet, and L. Deike. High-resolution direct simulation of deep water breaking waves : transition to turbulence, bubbles and droplets production. *Journal of Fluid Mechanics*, 942 :A27, 2022.

[17] F. Pierella, O. Lindberg, H. Bredmose, H. B. Bingham, R. W. Read, and A. P. Engsig-Karup. The derisk database : Extreme design waves for offshore wind turbines. *Marine Structures*, 80 :103046, 2021.

[18] P. Renaud, F. Hulin, M. Batlle Martin, Y.-M. Scolan, A. Tassin, N. Jacques, J. C. Harris, and J.-F. Filipot. Semi-analytical load models accounting for the tilt and motion of a cylinder impacted by a plunging breaking wave. In *Volume 2 : Structures, Safety, and Reliability*, International Conference on Offshore Mechanics and Arctic Engineering, page V002T02A021, 06 2023.

[19] V. Roeber and K. F. Cheung. Boussinesq-type model for energetic breaking waves in fringing reef environments. *Coastal Engineering*, 70(4) :1–20, 2012.

[20] B. R. Seiffert and G. Ducrozet. Simulation of breaking waves using the high-order spectral method with laboratory experiments : wave-breaking energy dissipation. *Ocean Dynamics*, 68 :65–89, 2018.

[21] C. E. Stringari and H. E. Power. The fraction of broken waves in natural surf zones. *Journal of Geophysical Research : Oceans*, 124(12) :9114–9140, 2019.

[22] M. L. Yates and M. Benoit. Accuracy and efficiency of two numerical methods of solving the potential flow problem for highly nonlinear and dispersive water waves. *Int. J. Numer. Meth. Fluids*, 77 :616–640, 2015.

[23] V. E. Zakharov. Stability of periodic waves of finite amplitude on the surface of a deep fluid. *J. Appl. Mech. Tech. Phys.*, 9(2) :190–194, 1968.